Radial Throw in Micromilling: A Simulation-Based Study to Analyze the Effects on Surface Quality and Uncut Chip Thickness

Sudhanshu Nahata
Department of Mechanical Engineering,
Carnegie Mellon University,
5000 Forbes Avenue,
Pittsburgh, PA 15213
e-mail: snahata@andrew.cmu.edu

Recep Onler
Department of Mechanical Engineering,
Carnegie Mellon University,
5000 Forbes Avenue,
Pittsburgh, PA 15213
e-mail: ronler@andrew.cmu.edu

O. Burak Ozdoganlar[1]
Department of Mechanical Engineering;
Department of Material Science and Engineering;
Department of Biomedical Engineering,
Carnegie Mellon University,
5000 Forbes Avenue,
Pittsburgh, PA 15213
e-mail: ozdoganlar@cmu.edu

This paper presents a simulation study toward analyzing the effect of radial throw in micromilling on quality metrics and on the deviation in tool-tip trajectory from its prescribed pattern. Both the surface location error (SLE) and the sidewall (peripheral) surface roughness are analyzed. The deviation in tool-tip trajectory is evaluated considering the flute-to-flute variations in the uncut chip thickness and changes in the tooth spacing angle. Radial throw indicates the instantaneous radial location of the tool axis, thereby capturing all salient features of tool-tip trajectory deviations, such as the general elliptical form of the radial motions. This is in contrast to the concept of run-out, which is a scalar quantity (total indicator reading) indicating the total displacement or change in the radial throw measured from a perfect cylindrical surface for one complete rotation of the axis. As such, measurement and analysis of radial throw is essential to understanding micromachining processes. In our previous work, we described an experimental approach for accurate determination of radial throw when using ultra-high-speed micromachining spindles. In this work, we present a simulation-based study to relate radial throw parameters and form to SLE, sidewall surface roughness, flute-to-flute variations of uncut chip thickness, and changes in tooth spacing angle for a two fluted micro-endmill. As expected, our study concludes that the magnitude, orientation, and form of radial throw all significantly affect the studied quality metrics, tooth spacing angle, and the flute-to-flute chip thickness variations. Specifically, the presence of radial throw with an elliptical form induces up to 50% variation in SLE, up to 20% variation in sidewall surface roughness, up to 60% variation in tooth spacing angle deviations, and up to 50% variation in flute-to-flute chip thickness. As such, the presented simulation approach can be used to assess the direct (kinematic) effects of the radial throw parameters on the quality metrics and chip thickness variations. [DOI: 10.1115/1.4043176]

Keywords: micromachining, micromilling, run-out, radial throw, surface generation, surface location error

Introduction

As per the ISO 230-7:2015 standards, radial throw of a rotating axis is defined as "distance between the geometric axis of a part (or test artifact) connected to a rotary axis and the axis average line, when the two axes do not coincide" [1]. The radial throw of tool-axis causes the trajectory of the cutting edges to deviate from the ideal trajectory, which is circular with a diameter equal to the tool diameter. As such, radial throw directly affects the kinematic position of the cutting edges, and thus, have a critical effect on the attainable precision in a machining process [2–4]. Unlike run-out, which indicates the *total* displacement of a rotating surface within a full rotation (measured by a stationary displacement sensor), the radial throw of tool-axis describes the *instantaneous* position of the tool-axis, and thus, depends on the rotation angle [1,5,6]. In other words, run-out is a time- and orientation-invariant constant value that is equal to the total indicator reading, whereas radial throw provides the location of the tool-axis in the cutting plane as a function of the rotation angle. Therefore, run-out only considers the magnitude of radial throw along a single measurement direction within a revolution but disregards the effect of the rotation angle. As such, radial throw accurately captures the kinematic trajectory of the tool-axis.

The radial throw alters the kinematic tool-tip trajectory, and thus, directly affects the dimensional error (surface location error, SLE) and sidewall (peripheral) surface roughness of a machining process. In addition, radial throw alters the chip thickness experienced by each cutting edge, thereby causing changes in both machining kinematics and dynamics, and inducing an indirect change to quality parameters. Therefore, it is essential to assess the effects of radial throw on quality metrics of a machining process.

Radial throw at the tool-tip arises from many factors such as tool-attachment errors [5,7], inherent spindle error motions [7–10], and dynamic response to excitations from a rotating unbalance [1,11,12]. Radial throw is described by a magnitude and an orientation, both of which can change with the rotation angle. Although the actual trajectory can contain many harmonics of the spindle frequency, the overall form is dominated by the motions at the spindle rotational frequency (i.e., the fundamental component or one-per-rev motions) [1,5,6,11,13]. In general, those motion follow an elliptical pattern. This elliptical form arises mainly from the structural (stiffness) asymmetry [1,11] and affects the quality metrics. If stiffness at the tool base (including spindle and other system-component stiffnesses) is perfectly

[1]Corresponding author.

Contributed by the Manufacturing Engineering Division of ASME for publication in the JOURNAL OF MICRO- AND NANO-MANUFACTURING. Manuscript received November 12, 2018; final manuscript received March 10, 2019; published online April 11, 2019. Assoc. Editor: Lawrence Kulinsky.

axisymmetric, then the form becomes circular. Thus, it is important to study the effects of varying radial throw magnitude and orientation as well as the unique effects of the more general elliptical radial throw trajectory.

Although radial throw has not been thoroughly studied in the literature, the effect of tool-tip run-out during micromachining has been analyzed in several works [13,14–22]. Most studies focus on surface generation as a function of spindle speed, feed rate, and tool geometry with little emphasis on radial throw magnitude and orientation. Zhang et al. [20] studied the effect of varying run-out length and angle to explore the single-edge cutting criteria. Liu et al. [15] showed that the peripheral surface roughness increased with run-out at higher feed rates. However, since run-out does not contain information about the radial throw orientation, the effects of orientation were not considered in their work. No study to date has considered the effect of elliptical form of the radial throw in quality metrics and chip-thickness variations.

In this work, a time-domain (kinematic) simulation of the micromilling process in the presence of radial throw is created, and the simulation is used to relate the radial throw parameters and form to the surface location error, peripheral surface roughness, and uncut chip thickness variations. The tool-tip trajectories for different radial throw form, magnitude, and orientation are considered, and the full-immersion (slot) milling process kinematics is simulated to determine the aforementioned quality metrics, the effective chip thickness, and the variations in the tooth spacing angle.

Model Development

Radial Throw in Micromilling. Figure 1 describes the one-per-rev component of the radial throw $\boldsymbol{\rho}(z,\theta)$ in a plane perpendicular to the average location of tool-axis [5]. In a full revolution, the one-per-rev radial throw causes the tool axis to follow an elliptical trajectory and alters the effective radii of the cutting edges. In the absence of radial throw, the tool axis would be shown as a point at O_z, and the cutting edges would follow a circular pattern with a radius equal to the tool radius r. The trajectory of the mth cutting edge in a given axial plane z is expressed by the vector $\boldsymbol{p_m}$ as

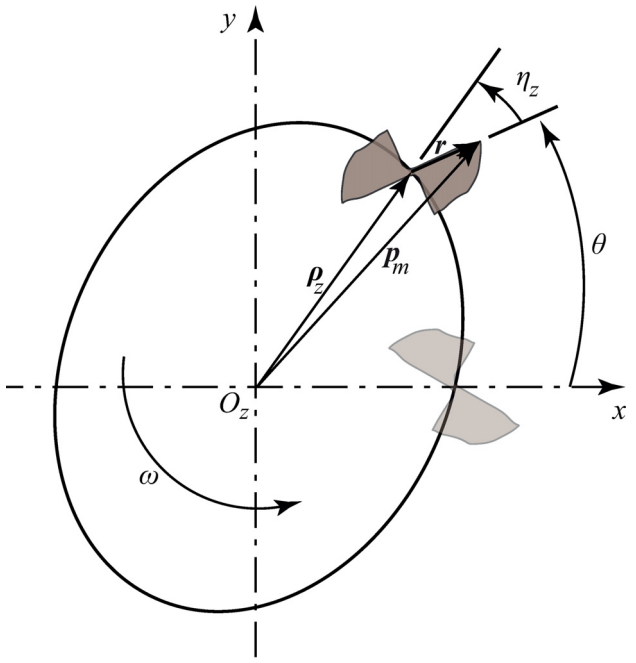

Fig. 1 Description of radial throw magnitude $\rho_z(\theta)$ and radial throw orientation $\eta_z(\theta)$. The one-per-rev component of radial throw with its general elliptical trajectory is shown. The radial throw magnitude is significantly exaggerated with respect to the micro-endmill diameter for illustration purposes.

$$\boldsymbol{p_m}(z,\theta) = (\rho_x(z,\theta) + r\cos(\theta + 2\pi(m-1)/n))\boldsymbol{i} + (\rho_y(z,\theta) + r\sin(\theta + 2\pi(m-1)/n))\boldsymbol{j} \quad (1)$$

where $\boldsymbol{i}$ and $\boldsymbol{j}$ are the unit vectors along the x and y directions, respectively. Here, ρ_x and ρ_y are the x and y components of the radial throw, θ is the rotation angle, and n is the total number of cutting edges (flutes). The orientation of radial throw is defined by $\eta_z(\theta)$, referenced with respect to the first (arbitrary chosen) cutting edge of the tool.

Modeling Approach. The trochoidal trajectory of the cutting edges is generated using Eq. (1) for a given cutting plane (axial position of the tool). This equation considers only the kinematics of the cutting process and does not include static or dynamic effects from the process mechanics or dynamics. In other words, *by definition*, the radial throw calculations exclude the effects of cutting forces, minimum chip thickness, elastic recovery, cutting-force related tool deflections, etc., and only determine the kinematic trajectory of the tool. Based on this definition, geometric imperfectness of the cutting tool also contributes to the radial throw. However, in this work, we considered a perfect tool without manufacturing errors or edge serrations, which could be on the order of the uncut chip thickness [23]. If those irregularities are known quantitatively, they can be straightforwardly captured in our approach.

In this work, we simulated a full-immersion milling process. For each slice (z position) of the tool, the points participating in the creation of the sidewall are used to calculate the channel width and sidewall surface roughness (see Fig. 2) The difference between the mean channel width and the prescribed width (which is equal to the tool diameter) is calculated as the dimensional error, half of which equals to SLE by definition. The average surface roughness (Ra) is calculated around the mean line (of the side profile) for both the up-milling and down-milling sides. To obtain the uncut chip thickness, an approach similar to that described in Ref. [24] is adopted: the uncut chip thickness is continuously monitored as a function of the rotation angle for both the cutting edges.

A two-fluted micro-endmill with 254 μm tool diameter and 30 deg helix angle is considered for the simulations. Since the radial throw magnitude and orientation both change with the axial location and the rotation angle (see Fig. 9(*a*)), many axial slices of the tool are involved in the creation of the sidewall, and the simulations can take into account the entire depth of cut in calculating quality metrics. However, for ease of presenting and understanding the effects of radial throw, results from a single axial slice are first presented. The quality parameters for the entire sidewall (for all axial slices combined) are then discussed.

Simulation Parameters. The simulation parameters (see Table 1) are selected to capture the contrast between the circular

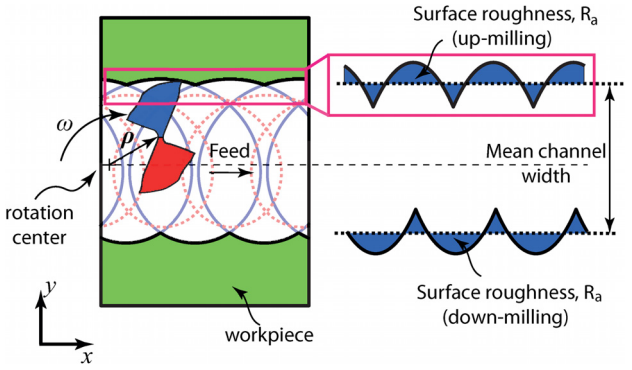

Fig. 2 The trochoidal tool-tip trajectory in the presence of radial throw ρ, and the parameters for calculation of the associated output metrics

and elliptical radial throw trajectories as well as to study the effects of varying radial throw magnitude and orientation. It is noted that the selected parameters are physically reasonable and reflect the previous measurements presented in the literature [5,7,23]. A constant feed rate of 5 μm/flute is chosen and it is prescribed along the x direction. Both the circular and the more general elliptical form of radial throw are analyzed. The magnitude of radial throw is varied between 0 and 15 μm for the circular form (elliptical ratio = 1). For the elliptical form, since the magnitude is a function of the rotation angle (see Fig. 1 on how $\boldsymbol{\rho}_z$ changes as a function of θ), the length of semiminor axis is kept fixed at 10 μm and the length of semimajor axis is kept fixed at 15 μm (elliptical ratio = 1.5, see Fig. 3). The feed direction is kept constant along the x axis. The orientation of the major axis of the ellipse—*the ellipse inclination angle*, θ_{ia}—measured in the counter-clockwise direction from the x axis, is varied from 0 to 180 deg. Since for both circular and elliptical forms, a fourfold symmetry exists in radial throw orientation for a two-fluted cutting tool, the radial throw orientation is only varied from 0 to 90 deg. For a given axial slice, the orientation of radial throw also varies within a revolution for an elliptical trajectory as the radial throw vector rotates at an angular speed different from the rotational speed of the cutting tool (see Fig. 1, where θ is measured with respect to the vector $\boldsymbol{r}$, rotation speed of which is different from that of $\boldsymbol{\rho}_z$). For the elliptical ratio of 1.5, the peak variation in radial throw orientation is found to be 11.5 deg within a revolution. Although this effect is captured in the simulation, we indicate only the radial throw orientation value prescribed at $\theta = 0$ deg.

Results and Discussion

Surface Location Error. Figure 4(*a*) depicts SLE (in μm) as a function of the radial throw magnitude and orientation for the circular form (elliptical ratio = 1). The SLE increases with an increase in radial throw magnitude and a steep change is observed when the radial throw orientation is closer to 0 deg. This is expected since, for a two-fluted cutter, for the 0 deg or 180 deg orientations, the radial throw vector is aligned with one of the cutting edges, thus directly increasing the *effective* tool radius experienced by that cutting edge. For the 90 deg orientation, however, the radial throw vector is perpendicular to the cutting edges, resulting in an effective radius very close to the actual tool radius.

Figure 4(*b*) presents SLE for different radial throw orientations and ellipse inclination angles for a fixed elliptical form (elliptical ratio = 1.5). Again, close to the 0 deg orientation, the effects of the elliptical form are pronounced. Specifically, the SLE varies by as much as 6 μm as the ellipse inclination angle is varied from 0 deg to 180 deg. For the 0 deg and 180 deg ellipse inclination angles, the major axis of the ellipse is oriented along the feed direction. Therefore, the effect of radial throw on the SLE is smaller as compared to other elliptical inclinations such as for the 90 deg inclination, where the major axis is perpendicular to the feed direction. In the vicinity of the 90 deg ellipse inclination angle (e.g., at 45 deg radial throw orientation), the SLE is marginally larger for inclination angles less than 90 deg when compared to the inclination angles greater than 90 deg. This is true for radial throw orientations between 0 and 90 deg as the radial throw vector makes an acute angle with the cutting edges, resulting in an increased magnitude of the effective tool radius. These results indicate the importance of considering the magnitude, orientation, and the form of radial throw to understand its effect on the process output.

Table 1 Parameters used in the time-domain simulations (unless stated otherwise)

Parameter	Value
Tool diameter (μm)	254
Feed rate (μm/flute)	5
Elliptical ratio	1, 1.5
Radial throw magnitude (μm)	0–15
Radial throw orientation (deg)	0–90
Ellipse inclination (deg)[a]	0–180

[a]For elliptical radial throw trajectory only.

Sidewall Surface Roughness. Figures 5(*a*) and 5(*b*) give the variation in the peripheral surface roughness (for the up-milling side) for the circular and elliptical forms, respectively. In Fig. 5(*a*), the surface roughness marginally decreases for an increase in the radial throw magnitude and for a decrease in the orientation of the radial throw. This is because the surface roughness decreases as the effective radii increase due to marginal decrease in the cusp heights. For very small radial throw magnitudes (<0.5 μm) or for radial throw orientations close to 90 deg, where both cutting edges participate in generating the sidewalls, the surface roughness is considerably lower. In general, the surface roughness is inversely related to the SLE when only one of the cutting edges participates in the sidewall surface generation.

For the elliptical form, as shown in Fig. 5(*b*), the notion of effective radii fails to explain the peripheral surface roughness as the trochoidal trajectories become complicated as compared to those for the circular form. For example, although at the 0 deg radial throw orientation, the effective radii at the 0 deg ellipse inclination angle are higher than those at the 90 deg inclination angle, the surface roughness shows the opposite trend. This is because an increase in effective radii no longer results in a guaranteed decrease in the cusp heights. For an elliptical form, the distance between the rotation center and the tool-center varies with the rotation angle, which, in turn, varies the effective radii as the tool rotates. The effect of this variation in the effective radii in the generation of peripheral surface is relatively difficult to imagine (specially for the tools with smaller tool diameter) and requires a time-domain simulation to clearly observe. However, when the trajectories are sketched, it becomes apparent how it may affect the surface roughness of the up-milling or the down-milling surfaces. For example, at the 45 deg radial throw orientation, the cusp heights are smaller at both the 30 deg and 120 deg ellipse inclination angles than those at the 90 deg inclination. This results in a higher surface roughness at the 90 deg inclination than that at the 30 deg and 120 deg inclinations. Thus, the contour plots play an important role in assessing the surface roughness variations for given combination of parameter. From Fig. 5(*b*), it can be observed that, for a fixed radial throw magnitude, the effect of radial throw orientation and/or ellipse inclination angle is found to vary surface roughness by up to 20%.

Similarly, Figs. 5(*c*) and 5(*d*) plot the peripheral surface roughness variation for down-milling cases. The trends are similar to the up-milling cases; however, the interaction between the radial throw and trochoidal path causes the roughness to be higher for down-milling cases, as expected.

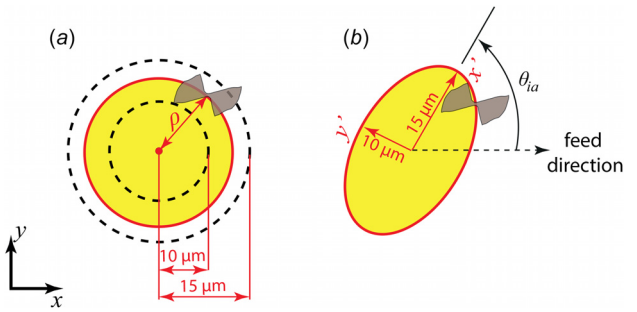

Fig. 3 Description of various forms (trajectories) of radial throw discussed in the text (*a*) circular and (*b*) elliptical. θ_{ia} is the inclination angle of the ellipse with respect to the feed direction.

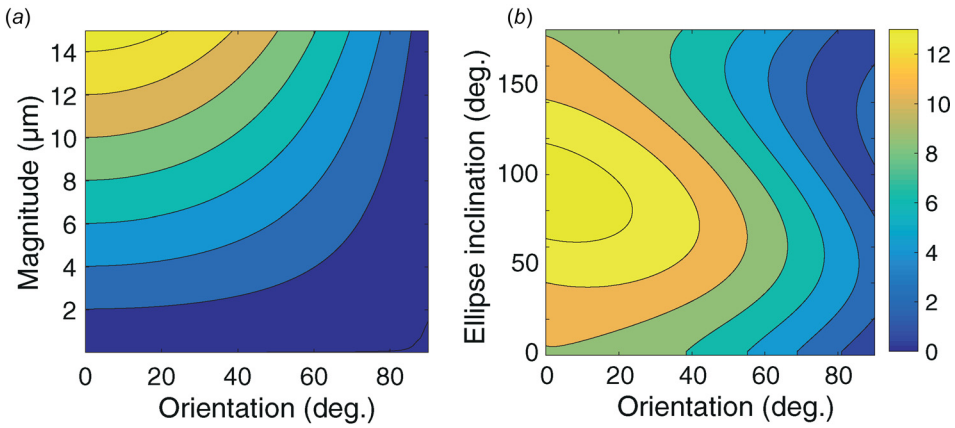

Fig. 4 SLE (in μm) for (*a*) varying radial throw magnitude and orientation for *circular* radial throw and (*b*) varying radial throw orientation and ellipse inclination angle for *elliptical* (fixed elliptical ratio) radial throw

Uncut Chip Thickness. Uncut chip thickness dictates many aspects of a milling process, including cutting forces, cutting mechanism (shearing or plowing), milling dynamics and stability, and tool wear [25–27]. Radial throw causes the dictated kinematic trajectory of the cutting edges to vary and to become nonuniform, inducing axial-location dependent variations in chip thicknesses experienced by different cutting flutes. A sample case included in Fig. 6 demonstrates the uncut chip thicknesses as it is experienced by the first (#1) and the second (#2) cutting edges at different radial throw orientations when the radial throw has a *circular form*. For this simulation, the magnitude of radial throw is kept fixed at 2.5 μm, which is half the prescribed feed rate of 5 μm. In the absence of radial throw, both cutting edges would experience the same chip-thickness profile with a 180 deg separation. When radial throw is present, the uncut chip thickness profiles are significantly affected by the radial throw and its orientation. As discussed earlier, when the radial throw orientation is 90 deg, for a circular radial throw form, the chip thicknesses are minimally affected by the radial throw. However, as the orientation deviates from 90 deg, one of the cutting flutes increasingly experiences a larger chip thickness than the other. The most severe effect occurs when the orientation is sufficiently close to 0 deg or 180 deg: only one of the two cutting edges participates in cutting. As a result, the cutting forces would vary considerably from flute to flute, and the uneven chip thicknesses would also cause increased wear on one of the cutting edges, resulting in shortened tool life. Of

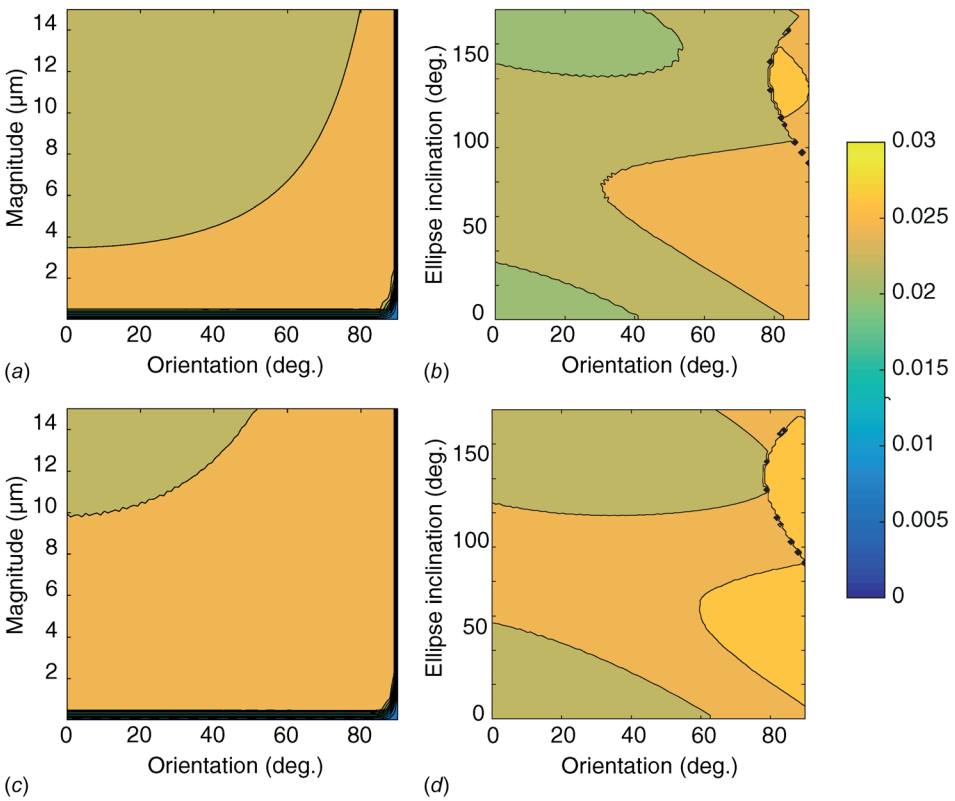

Fig. 5 Peripheral surface roughness for ((*a*) and (*b*)) up-milling and ((*c*) and (*d*)) down-milling cases. (*a*) and (*c*) are for a circular trajectory with varying radial throw magnitude and orientation, and (*b*) and (*d*) are for an elliptical (fixed elliptical ratio) trajectory with varying radial throw orientation and ellipse inclination angle. The Ra is in μm.

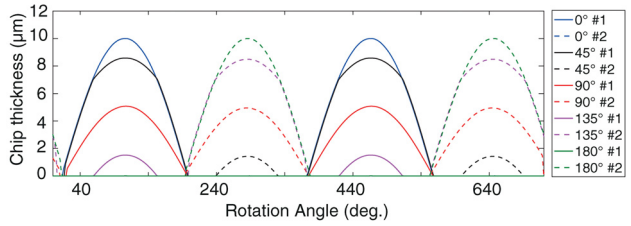

Fig. 6 Uncut chip thickness variations for a circular radial throw trajectory at a fixed radial throw magnitude of 2.5 μm and at varying radial throw orientations. A two-fluted tool is considered. Each radial throw orientation is listed on the right column, and the cutting edges #1 and #2 are represented by solid and dotted lines, respectively. Note that the ideal case (in the absence of radial throw) would be similar to the 90 deg radial throw orientation case (the readers are referred to the web version of the paper for clear interpretation).

course, additional effects would be expected when mechanics (including elastic recovery and quasi-static forces) and dynamics (including forced vibrations and tool deflections) are included, the effect of radial throw could be considerably exacerbated.

Figures 7(*a*) and 7(*b*) present uncut chip thickness for an *elliptical form* of radial throw at 0 deg and 90 deg radial throw orientations, respectively. Each subplot features uncut chip thickness profiles for different ellipse inclination angles ranging from 0 to 180 deg for the cutting edges #1 and #2. For radial throw orientation of 90 deg in Fig. 7(*a*) (favorable case from Fig. 6), depending on the ellipse inclination angle, the maximum chip thickness between the two flutes was seen to vary by up to 50% (e.g., 4 μm/flute at 45 deg versus 6 μm/flute at 135 deg). Such variations can cause significant changes in the cutting-force profiles. Therefore, it is critical to understand the effects of both the magnitude and the orientation of radial throw as well as the effects of ellipse inclination angle in the case of elliptical form.

Tooth Spacing Angle. In the absence of radial throw, the tooth spacing angle is 360/n deg, where n is the number of flutes. Radial throw causes the tooth spacing angle to deviate from 360/n deg. For a two-fluted tool, the deviation becomes maximum when the radial throw orientation is 90 deg and becomes zero for 0 deg radial throw orientation. This deviation in the tooth spacing angle $\Delta\theta_p$ (see Fig. 8(*a*) for a visual description) can be described as

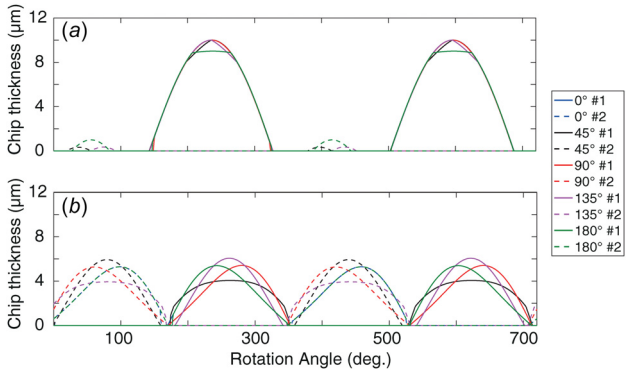

Fig. 7 Uncut chip thickness variation for an elliptical trajectory fixed at a semimajor and a semiminor axis of 3 μm and 2 μm, respectively. The ellipse inclination angle is varied for radial throw orientations of (*a*) 0 deg and (*b*) 90 deg. Each ellipse inclination angle is listed on the right column, and the cutting edges #1 and #2 are represented by solid and dotted lines, respectively (the readers are referred to the web version of the paper for clear interpretation).

$$\Delta\theta_p = 2\cos^{-1}\frac{(2r)^2 - r_1^2 - r_2^2}{2r_1 r_2} \tag{2}$$

where r is the tool radius, and r_1 and r_2 are the effective radii for cutting edges #1 and #2 in the presence of radial throw $\boldsymbol{\rho}$, respectively.

As can be deduced from Eq. (2), the change in tooth spacing angle is a function of the tool radius as well as the magnitude and orientation of radial throw, resulting in two different effective radii. As the tool diameter decreases, higher deviations in tooth spacing angles are expected since the effective radii in the presence of a given radial throw become farther apart in magnitude.

Figure 8(*b*) shows how the tooth spacing angles change with the radial throw magnitude and orientation for a *circular trajectory*. As expected, the variations are higher when radial throw orientation approaches 90 deg. On the other hand, the deviation of tooth spacing angle in the elliptical form of radial throw is more complex since the magnitude of radial throw becomes a function of the rotation angle. Figure 8(*c*) shows the deviation in the tooth spacing angle with varying radial throw orientation and ellipse inclination angle for an elliptical form (elliptical ratio = 1.5), when the radial throw vector is aligned in the feed direction. When the orientation of radial throw is set at 90 deg, which is favorable for minimizing SLE, a significantly higher variation (up to 60%) in the tooth spacing angle is observed as the ellipse inclination angle is varied from 0 to 180 deg. A similar effect is observed at other orientations as well: for instance, at 45 deg radial throw orientation, the deviation in tooth spacing angle decreases when the minor-axis of the ellipse comes closer to the feed direction (ellipse inclination angles between 50 and 130 deg). Again, similar to the SLE plots, the asymmetry in the vicinity of 90 deg inclination is a result of the acute angle between the radial throw vector and the cutting-edges. This is a direct effect of the local increase in the magnitude of radial throw seen in the elliptical form, resulting in changes in the effective radii. Because of these deviations in the tooth spacing angle, the orientation of cutting geometry is considerably affected, including changes in rake angle and the side clearance angle. The significant changes in the tooth spacing angle cause the rake angle for one cutting edge to decrease, and the rake angle for the other cutting edge to increase by the same amount. This could result in significant differences in material removal mechanism, cutting forces, and tool life [28,29].

Effect of Depth of Cut. So far, we have only considered a single axial slice of the tool and its interaction with the workpiece, where the radial throw orientation remains constant for a particular case. When the depth is considered, both the magnitude of the radial throw of the tool axis (due to the tool tilt) and the reflection of the radial throw at each cutting point (due to the pretwist of the flutes) will vary along the axis of the tool. Therefore, for a given axial slice, both the magnitude and the orientation of the radial throw (as it is determined in reference to a cutting edge) will vary. This is illustrated in Fig. 9(*a*) for a 50 μm depth of cut using a 254 μm diameter tool (with a 30 deg helix angle): a 6.5 deg change in radial throw orientation is calculated. Similarly, for the tool diameters of 50.8 μm and 508 μm with a constant helix angle of 30 deg, a 50 μm depth of cut corresponds to a 32.5 deg and 3.25 deg change in radial throw orientation, respectively.

To some extent, the effect of radial throw parameters and form can be evaluated from the analysis presented earlier. In essence, due to the helix angle, different tool slices will experience different radial throw orientations. Furthermore, the presence of tilt will vary the radial throw magnitude with the axial location z, although this variation is commonly small for regular- and stub-length microtools. Considering these, the entire sidewall surface can be generated for a given depth of cut, and the areal surface roughness of the sidewall and the average SLE can be calculated. Furthermore, the chip thickness variations at any axial slice of the tool can also be calculated. An example case is presented in Fig. 10,

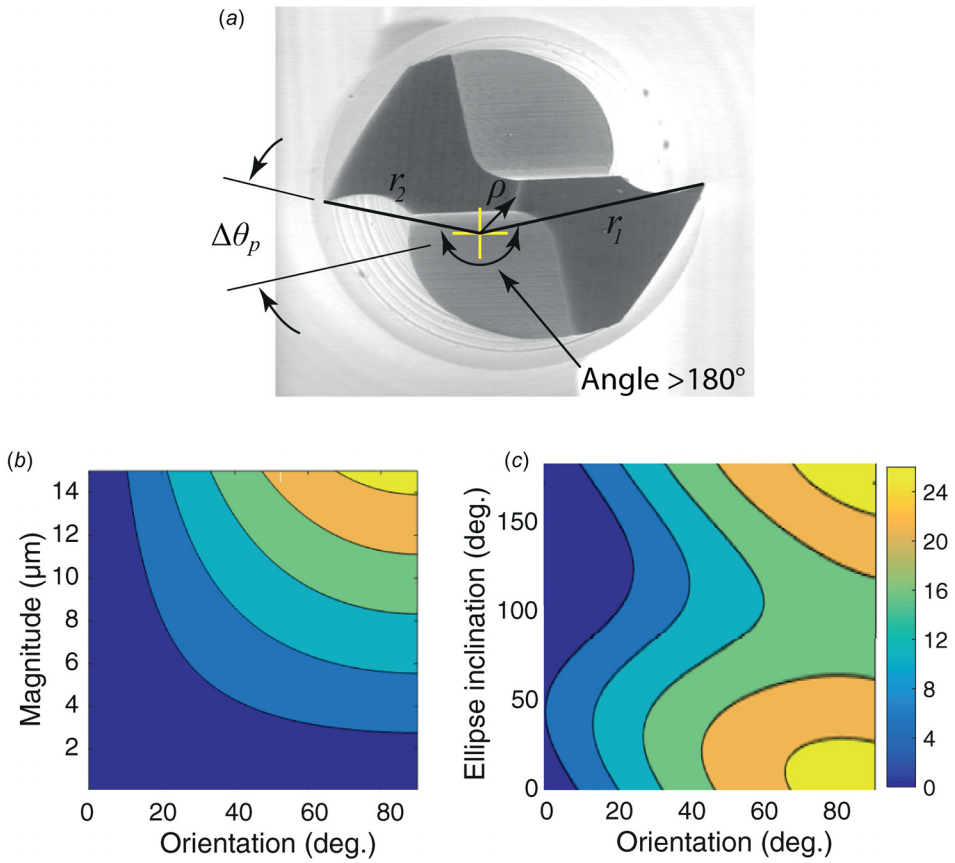

Fig. 8 (*a*) The description of deviation in the tooth-spacing angle $\Delta\theta_p$ for (*b*) varying magnitude and orientation of radial throw for a circular trajectory, and (*c*) varying radial throw orientation and ellipse inclination angle for an elliptical ratio of 1.5 (from Table 1) The unit is deg

where the sidewall surfaces generated by the up-milling and the down-milling action are shown in Figs. 10(*b*) and 10(*c*), respectively. For this case, we used a 254 μm tool with 30 deg helix angle and assumed a circular form of radial throw with a constant magnitude of 15 μm (absence of tool-tilt) and an orientation of 0 deg at the tool-tip. Figures 10(*d*) and 10(*e*) show the lateral translation (in x) of the cusps with z (indicated by nonvertical arrows) because of the finite helix angle of the cutting tool. It is noted that we expect the cusp heights to change (y-axis) with depth (z-axis) due to the changes in radial throw orientation ($\Delta\eta$) of the tool cutting points at different depths (highlighted in Fig. 11). When the tool-tilt is included, it will result in a finite change along the magnitude axis ($\Delta\rho$) at different depths. The cumulative effect of both results in a finite set of points in Fig. 9(*b*) which can be averaged to calculate the average SLE for the whole channel. For example, the SLE for the simulated channel in Fig. 10(*a*) is calculated to be 9.22 μm (also shown in Fig. 11) which is equivalent to taking an average of SLE's

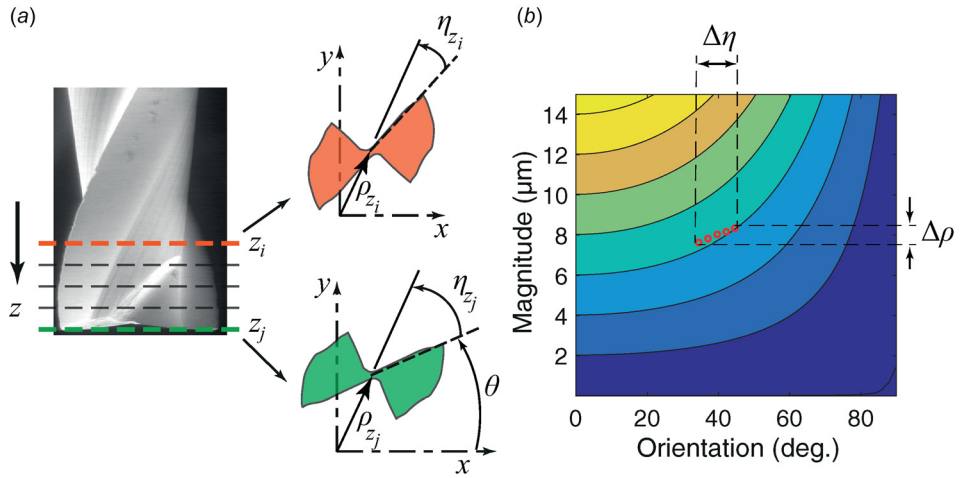

Fig. 9 (*a*) A change in radial throw orientation with change in axial position (indicated by *z*) arising from the helical flutes and (*b*) the effect of a finite depth of cut results in a variable magnitude (effect of tool-tilt) and variable orientation of radial throw (effect of helix angle), highlighted by red circles (the readers are referred to the web version of the paper for clear interpretation)

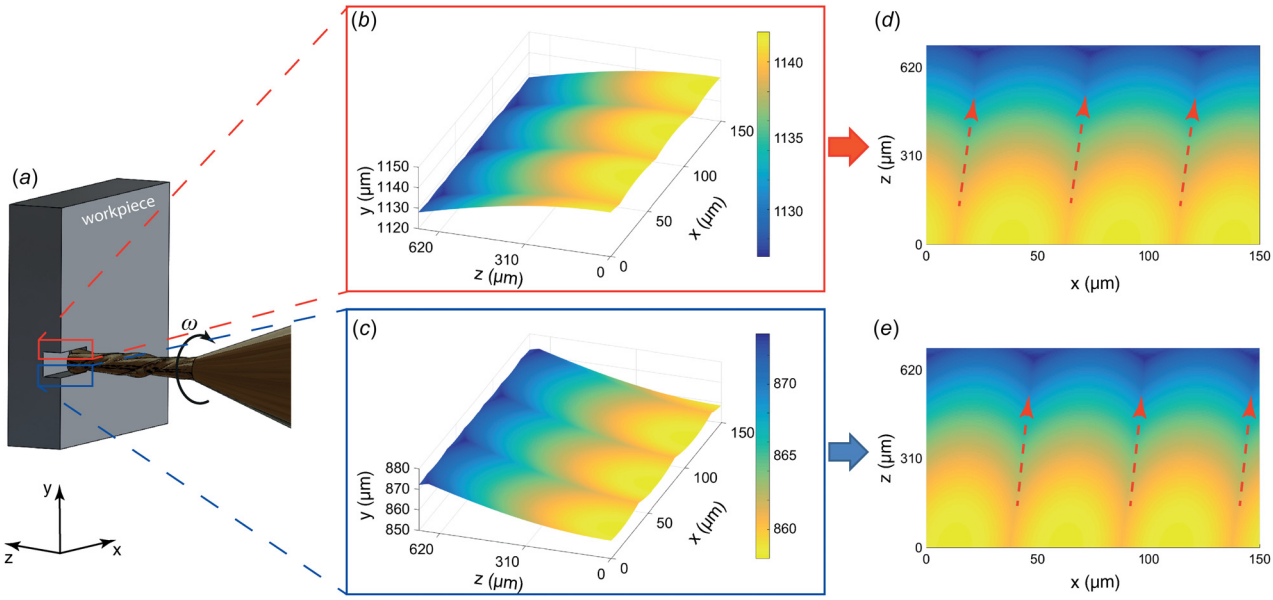

Fig. 10 (*a*) An example 3D surface generated by a 254 μm, two fluted micro-endmill (30 deg helix angle) at a feed of 25 μm/flute and depth-of-cut of 700 μm, (*b*) up-milling, and (*c*) down-milling. ((*d*) and (*e*)) The cusps also translate laterally (in *x*) with *z* (indicated by nonvertical arrows) because of the finite helix angle of the cutting tool. Note that the scales are different along different axes. A circular form of radial throw was assumed with a constant magnitude of 15 μm and an orientation of 0 deg at the tool-tip.

between 0 and 90 deg radial throw orientations at 15 μm radial throw magnitude (from Fig. 4(*a*)).

Summary and Conclusions

This paper presented a simulation of the kinematic trajectory of the cutting edges in the presence of radial throw to enable analyzing the effect of radial throw on micromachining quality and flute-to-flute chip-thickness variations.

Based on the set of parameters used in the simulations, the effect of radial throw on SLE was found to be significant, whereas its effect on *peripheral surface roughness* was found to be relatively insignificant for low feed rates. The *variation of uncut chip thickness* experienced by successive cutting flutes is seen to be strongly affected (up to 100%) by the orientation of radial throw for both circular and elliptical forms of radial throw. In addition, for an elliptical trajectory with 90 deg radial throw orientation, changes in ellipse inclination angles caused up to 50% variation in the uncut chip thickness. The deviations in the *tooth spacing angles* were found to be 60% higher for an elliptical form than that for the circular form. Importantly, when the radial throw form is elliptical, the effect of radial throw parameters became considerably more complex, making it impractical to arrive at the presented conclusions through intuition alone. These results show the importance of studying the radial throw magnitude, orientation, and form in understanding the micromilling process output.

The presented simulation effort derives results purely on the basis of the kinematics of the micromilling process. Clearly, without capturing mechanics and dynamics of the process, obtaining an accurate prediction of quality parameters through just the kinematics of the process is not possible (except for special circumstances, such as very low-strength workpiece, very stiff tool, and very low dynamic response at the given conditions). However, those predictions can provide important insights and guidelines, e.g., to facilitate comparisons between different cases. More importantly, the knowledge of kinematics (that is, the actual prescribed trajectory of the tool tip) is a prerequisite to capturing cutting mechanics and dynamics toward a comprehensive simulation of a micromachining process.

Overall, we conclude that the presented simulations and the associated analyses enable providing accurate description of cutting-edge trajectories and their implications on the process outcomes. The simulations also enable in effectively analyzing the contrasts between the circular and elliptical forms of radial throw. Our future work will expand the simulation framework by adding the cutting mechanics and machining dynamics aspects.

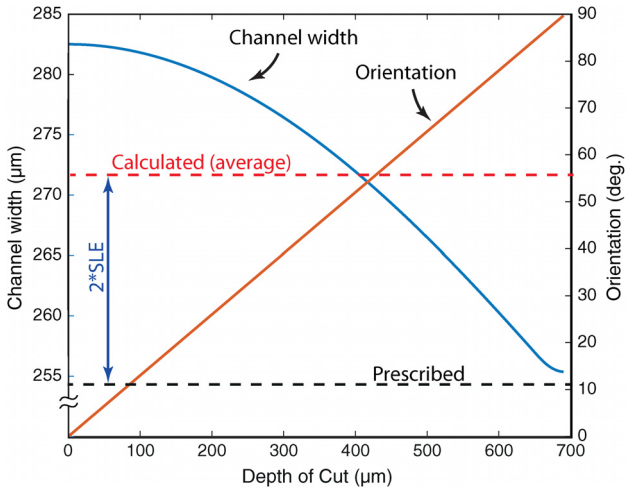

Fig. 11 The variation in channel width and radial throw orientation with depth of cut for the example case presented in Fig. 10. The prescribed width is 254 μm.

Funding Data

- National Institute of Standards and Technology (NIST) (Award No. #70 NANB12H208; Funder ID: 10.13039/100000161).
- National Science Foundation (Grant No. CMMI-1334402; Funder ID: 10.13039/501100008982).

Nomenclature

n = number of cutting edges
p = trajectory of cutting edge

r = tool radius
r_1 = effective tool radii #1
r_2 = effective tool radii #2
z = axial (xy) plane at a distance z from spindle nose
$\Delta\theta_p$ = tooth spacing angle deviation
η = orientation of radial throw
θ = rotation angle
θ_{ia} = ellipse inclination angle
ρ = magnitude of radial throw

References

[1] ISO, 2015, "Test Code for Machine Tools—Geometric Accuracy of Axes of Rotation," International Organization for Standardization, Vernier, Geneva, Switzerland, Standard No. ISO 230-7.
[2] Lee, K., and Dornfeld, D. A., 2004, "A Study of Surface Roughness in the Micro-End-Milling Process," Laboratory for Manufacturing and Sustainability, UC Berkele, Berkeley, CA (epub).
[3] Schmitz, T. L., Couey, J., Marsh, E., Mauntler, N., and Hughes, D., 2007, "Run-Out Effects in Milling: Surface Finish, Surface Location Error, and Stability," Int. J. Mach. Tools Manuf., **47**(5), pp. 841–851.
[4] Filiz, S., and Ozdoganlar, O. B., 2008, "Microendmill Dynamics Including the Actual Fluted Geometry and Setup Errors—Part II: Model Validation and Application," ASME J. Manuf. Sci. Eng., **130**, p. 31120.
[5] Nahata, S., Onler, R., Shekhar, S., Korkmaz, E., and Ozdoganlar, O. B., 2018, "Radial Throw in Micromachining: Measurement and Analysis," Precis. Eng., **54**, pp. 21–32.
[6] Nahata, S., Onler, R., Korkmaz, E., and Ozdoganlar, O. B., 2018, "Radial Throw at the Cutting Edges of Micro-Tools When Using Ultra-High-Speed Micromachining Spindles," Procedia Manuf., **26**, pp. 1517–1526.
[7] Anandan, K. P., and Ozdoganlar, O. B., 2013, "Analysis of Error Motions of Ultra-High-Speed (UHS) Micromachining Spindles," Int. J. Mach. Tools Manuf., **70**, pp. 1–14.
[8] Nahata, S., Anandan, K. P., and Ozdoganlar, O. B., 2013, "LDV-Based Spindle Metrology for Ultra-High-Speed Micromachining Spindles," North American Manufacturing Research Conference (NAMRC/SME), Madison, WI, June 10–14, pp. 2–7.
[9] Anandan, K. P., and Ozdoganlar, O. B., 2016, "A Multi-Orientation Error Separation Technique for Spindle Metrology of Miniature Ultra-High-Speed Spindles," Precis. Eng., **43**, pp. 119–131.
[10] Anandan, K. P., Tulsian, A. S., Donmez, A., and Ozdoganlar, O. B., 2012, "A Technique for Measuring Radial Error Motions of Ultra-High-Speed Miniature Spindles Used for Micromachining," Precis. Eng., **36**(1), pp. 104–120.
[11] Lu, X., Jamalian, A., and Graetz, R., 2011, "A New Method for Characterizing Axis of Rotation Radial Error Motion—Part 2: Experimental Results," Precis. Eng., **35**(1), pp. 95–107.
[12] Bediz, B., Arda Gozen, B., Korkmaz, E., and Burak Ozdoganlar, O., 2014, "Dynamics of Ultra-High-Speed (UHS) Spindles Used for Micromachining," Int. J. Mach. Tools Manuf., **87**, pp. 27–38.
[13] Kim, G. H., Yoon, G. S., Lee, J. W., Kim, H. K., and Cho, M. W., 2012, "A Study on the Micro-Endmilling Surface Prediction Model With Non-Dynamic Errors," Int. J. Precis. Eng. Manuf., **13**(11), pp. 2035–2041.
[14] Wang, W., Kweon, S. H., and Yang, S. H., 2005, "A Study on Roughness of the Micro-End-Milled Surface Produced by a Miniatured Machine Tool," J. Mater. Process. Technol., **162–163**, pp. 702–708.
[15] Liu, X., DeVor, R. E., and Kapoor, S. G., 2007, "Model-Based Analysis of the Surface Generation in Microendmilling—Part II: Experimental Validation and Analysis," ASME J. Manuf. Sci. Eng., **129**(3), p. 461.
[16] Jing, X., Tian, Y., Yuan, Y., and Wang, F., 2017, "A Runout Measuring Method Using Modeling and Simulation Cutting Force in Micro End-Milling," Int. J. Adv. Manuf. Technol., **91**(9–12), pp. 4191–4201.
[17] Attanasio, A., 2017, "Tool Run-Out Measurement in Micro Milling," Micromachines, **8**(7), p. 221.
[18] Chen, W., Huo, D., Teng, X., and Sun, Y., 2017, "Surface Generation Modelling for Micro End Milling Considering the Minimum Chip Thickness and Tool Runout," Procedia CIRP, **58**, pp. 364–369.
[19] Yuan, Y., Jing, X., Ehmann, K. F., and Zhang, D., 2018, "Surface Roughness Modeling in Micro End-Milling," Int. J. Adv. Manuf. Technol., **95**(5–8), pp. 1655–1664.
[20] Zhang, X., Pan, X., Wang, G., and Zhou, D., 2018, "Tool Run-Out and Single-Edge Cutting in Micro-Milling," Int. J. Adv. Manuf. Technol., **96**(1–4), pp. 821–832.
[21] Davoudinejad, A., Tosello, G., Parenti, P., and Annoni, M., 2017, "3D Finite Element Simulation of Micro End-Milling by Considering the Effect of Tool Run-Out," Micromachines, **8**(6), p. 187.
[22] Attanasio, A., Abeni, A., Özel, T., and Ceretti, E., 2019, "Finite Element Simulation of High Speed Micro Milling in the Presence of Tool Run-Out With Experimental Validations," Int. J. Adv. Manuf. Technol., **100**(1–4), pp. 25–35.
[23] Jun, M. B., DeVor, R. E., and Kapoor, S. G., 2006, "Investigation of the Dynamics of Microend Milling—Part II: Model Validation and Interpretation," ASME J. Manuf. Sci. Eng., **128**(4), pp. 901–912.
[24] Campomanes, M. L., and Altintas, Y., 2003, "An Improved Time Domain Simulation for Dynamic Milling at Small Radial Immersions," ASME J. Manuf. Sci. Eng., **125**(3), p. 416.
[25] Moges, T. M., Desai, K. A., and Rao, P. V. M., 2016, "Improved Process Geometry Model With Cutter Run-Out and Elastic Recovery in Micro-End Milling," Procedia Manuf., **5**, pp. 478–494.
[26] Malekian, M., Park, S. S., and Jun, M. B. G., 2009, "Modeling of Dynamic Micro-Milling Cutting Forces," Int. J. Mach. Tools Manuf., **49**(7–8), pp. 586–598.
[27] Liu, X., Jun, M. B. G., DeVor, R. E., and Kapoor, S. G., 2004, "Cutting Mechanisms and Their Influence on Dynamic Forces, Vibrations and Stability in Micro-Endmilling," ASME Paper No. IMECE2004-62416.
[28] Altintas, Y., 2012, *Manufacturing Automation: Metal Cutting Mechanics, Machine Tool Vibrations, and CNC Design*, Cambridge University Press, New York.
[29] Moges, T. M., Desai, K. A., and Rao, P. V. M., 2017, "On Modeling of Cutting Forces in Micro-End Milling Operation," Mach. Sci. Technol., **21**(4), pp. 562–581.